Spectroscopic properties of Er³⁺ doped germanate glasses before and after a heat treatment process

ARNAUD LEMIERE,[1,*] **BARTOSZ BONDZIOR,**[1,2]
LUUKAS KUUSELA,[1] **ALEXANDER VEBER,**[1]
AND LAETICIA PETIT[1]

[1]*Photonics Laboratory, Tampere University, Korkeakoulunkatu 3, Tampere, 33720, Finland*
[2]*Institute of Low Temperature and Structure Research, Polish Academy of Sciences, Okólna 2,50-422 Wrocław, Poland*
[*]*arnaud.lemiere@tuni.fi*

Abstract: In this paper structural, thermal and optical properties of Er³⁺ doped germanate glasses with the composition of $63.0GeO_2$-$9.8Ga_2O_3$-$11.1BaO$-$4.9X$-$8.8Na_2O$-$2.5Er_2O_3$ (in mol%), where $X = ZnO$, TiO_2, Al_2O_3 and Y_2O_3 are reported. The investigated glasses exhibit low phonon energies (<1000 cm^{-1}) and high glass transition temperature varying between 588 and 642 °C. The Raman spectra evidence about different polymerization degree of the glasses. The thermal treatment leads to the precipitation of various crystals, the composition of which depends on the glass composition. According to the spectroscopic properties Er³⁺ ions are suspected to have similar local environment in the as-prepared glasses. However, Er-doped crystals are expected to precipitate upon devitrification, which leads to significant change of the spectroscopic properties, in particular increase in the intensity of upconversion and MIR emissions is observed. It is demonstrated that the glasses with Y_2O_3, ZnO and TiO_2 are promising glasses especially for MIR applications.

1. Introduction

Luminescent materials have been of great interest in order to develop new light sources with different emissions in the visible, the near-infrared (NIR) and in the mid-infrared (MIR) spectral ranges [1–3]. Those light sources are needed in sectors such as medicine, environment, sensing, and bioengineering [4,5], especially because of the spectral signatures of many molecules which are located in 2.0-5.0 μm spectral region (transparency window of the earth atmosphere) [6]. Since Er³⁺ ions emit in NIR and MIR spectral regions, these ions have become of particular focus, especially because of their easy pumping at 980 nm. The visible emission of Er³⁺ ions is mainly due to three transitions of Er³⁺ ions: $^2H_{11/2} \rightarrow {}^4I_{15/2}$, $^4S_{3/2} \rightarrow {}^4I_{15/2}$, and $^4F_{9/2} \rightarrow {}^4I_{15/2}$. The NIR emission centered at ~1.5 μm is due to $^4I_{13/2} \rightarrow {}^4I_{15/2}$ transition of Er³⁺ ions while the MIR emission centered at ~2.7 μm is due to $^4I_{11/2} \rightarrow {}^4I_{13/2}$ transition. The probability of a radiative transition between $^4I_{11/2}$ and $^4I_{13/2}$ states is strongly improved in a glass matrix with low-phonon energy, in which the multiphonon nonradiative relaxation cannot deplete $^4I_{11/2}$ excited state [7].

Silica glass is not a promising material for light emission in the MIR region due to its high phonon energy, narrow transmission window compared to other glass systems [8] and low rare-earth solubility [9]. Therefore, many efforts have been made in the development of other glass systems emitting in the visible, NIR and MIR regions such as the fluoride [10,11], chalcogenide [12,13] and tellurite [14,15] networks. Glasses in the germanate system seem to

be especially promising because of their wide infrared transmission window [16], low phonon energy, and their good optical, chemical, and mechanical properties [17]. The composition of germanate glasses can be easily modified to improve specific properties; for example, ZnO, Al_2O_3 and Y_2O_3 can be added into the germanate network to increase the glass stability [18,19]. Due to the good rare-earth solubility, germanate glasses can be easily doped with high level of rare-earth ions such as Er^{3+} leading to the formation of glasses with upconversion, NIR and MIR luminescence when pumped at 980 nm [20].

Glass-ceramics have been of great interest as they can exhibit improved spectroscopic properties as compared to parent glass if the rare-earth ions are located in specific crystals after the devitrification. A glass-ceramic is a material containing both a crystalline phase and a glassy phase, allowing to add the crystal-like spectroscopic characteristics to a glassy material. Pisarska *et al*. [21] demonstrated a significant improvement of the upconversion from the Er^{3+} doped glass with the composition $39.5PbO-10PbF_2-50GeO_2-0.5ErF_3$ (mol%) after a heat treatment at 675 °C during 5 h due to the formation of Er^{3+}-doped PbF_2 crystals. Kang *et al*. [22] showed an enhanced intensity of the luminescence at 1.55 µm after a heat treatment between 400 and 640 °C for 8 h of the $59GeO_2-8TiO_2-8BaO-22Li_2O-3Er_2O_3$ (mol%) glass due to the formation of Li_2GeO_3 and $BaTiO_3$ crystals. An enhancement of the emission intensity at 2.7 µm was reported after heat treating the $50GeO_2-10Ga_2O_3-12NaF-25BaF_2-2.9LaF_3-0.1ErF_3$ (mol%) glass at 550 °C for 10 h due to the formation of Ba_2LaF_7 and BaF_2 crystals. [23]. These studies, taken as examples, clearly show the potential of glass-ceramics as compared to parent glasses. However, to the best of our knowledge, there have been fewer studies reported on germanate glass-ceramics compared to silicate based glass-ceramics for example.

In this work we report the preparation and characterization of new Er^{3+}-doped germanate glasses and glass-ceramics. The impact of the glass composition on the physical, thermal, structural, optical, and spectroscopic properties of the glass is investigated in order to develop glasses with improved spectroscopic properties. The glasses are heat treated to grow crystals in the glasses and the impact of the crystallization on the spectroscopic properties of the glasses is discussed.

2. Experimental procedures

2.1. Samples preparation

Glasses with the composition $63.0GeO_2-9.8Ga_2O_3-11.1BaO-4.9X-8.8Na_2O-2.5Er_2O_3$ (in mol%), where X = ZnO, TiO_2, Al_2O_3 and Y_2O_3 (labeled as GeZn, GeTi, GeAl and GeY, respectively) are prepared using the standard melt-quenching method and in the same week to avoid any changes in the atmosphere relative humidity or changes in the furnaces capabilities. Therefore, the condition preparations are similar for each glasses. The batches are prepared using GeO_2 (Sigma-Aldrich, 99.99%), Ga_2O_3 (Sigma-Aldrich, 99.99%), BaO (Sigma-Aldrich, 99.99%), Na_2CO_3 (Sigma-Aldrich, 99.8%), Er_2O_3 (Sigma-Aldrich, 99.99%), ZnO (Sigma-Aldrich, 99.99%), TiO_2 (Sigma-Aldrich, 99.8%), Al_2O_3 (Sigma-Aldrich, 99%), and Y_2O_3 (Sigma-Aldrich, 99.9%) as the raw materials. The 10 g batches are prepared and mixed using a mortar to obtain a homogenous mixture. The mixture is transferred in a platinum (Pt) crucible and melted at 1450 °C (for GeAl and GeZn) or at 1550 °C (for GeTi and GeY) with a ramp of 15 °C/min after a decarbonation step of 30 min at 450 °C. After 40 min at the melting temperature, the melt is quenched on a brass plate and finally annealed at 40°C below the glass transition temperature of the glasses for 5 h and cooled slowly to release the internal stress from the glass. Finally, the glasses are heat treated at 20 °C above the glass transition temperature (T_g) for 17 h and at the crystallization temperature (T_p) for 1, 6 and 12 h in order to grow crystals. Undoped glasses have also been prepared specifically for Raman measurements.

2.2. Physical and thermal properties

The density of the glasses is measured by the Archimedes' method. Ethanol is used as immersion liquid and results are obtained with an accuracy ± 0.02 g/cm^3.

The thermal properties of the glasses, T_g and T_p are measured using differential thermal analysis (DTA, Netszch JUPITER F1 instrument). The measurements are carried out in a Pt crucible using a heating rate of 10 °C/min. The T_g is determined as the inflection point of the endotherm peak obtained by taking the first derivative of the DTA curve, while T_p is taken at the maximum of the exothermic peak. The onset of the crystallization peak, T_x, is also measured, providing information about the glass thermal stability, $\Delta T = T_x - T_g$. All measurements are performed with an accuracy of ± 3 °C.

2.3. Optical properties

The absorption spectra are measured using UV–Vis–NIR spectrophotometer (UV-3600 Plus, Shimadzu) from 250 to 1800 nm. The absorption cross-section σ_{abs} (λ) is calculated using Equation (1):

$$\sigma_{abs}(\lambda) = \frac{2.303 \log(I_0/I)}{L \times N_{Er^{3+}}} \tag{1}$$

where log (I_0/I) is the absorbance, L is the thickness of the sample (in cm) and N_{Er}^{3+} is the concentration of rare-earth ions (ions/cm^3). The accuracy of absorption cross-section is $\pm 10\%$.

The IR spectra were measured using a PerkinElmer Spectrum One FTIR (Fourier-transform infrared spectroscopy) spectrometer in transmission mode from 1000 cm^{-1} to 5000 cm^{-1}.

2.4. Structural properties

The Raman spectra of the glasses are acquired with a Renishaw inVia Qontor Raman microscope equipped with a cooled charge coupled device (CCD) camera using a 405 nm laser for the excitation. The spectra are normalized to the maximum intensity band; therefore all the intensity changes shown/observed are relative to the main peak. The measurements are taken for Er^{3+} free glasses to avoid luminescence of the rare-earth ion.

2.5. Spectroscopic properties

The upconversion (UC) and NIR emission spectra of the samples are measured in the 500-800 nm and 1400–1700 nm ranges, respectively, using a continuous-wave 980 nm monochromatic single-mode fiber pigtailed laser diode (CM962UF76P-10R, Oclaro) for excitation. The spectra are acquired using a Spectro 320–131 optical spectrum analyzer (OSA, Instrument Systems Optische Messtechnik GmbH). The MIR emission spectra are measured in the range 2500-3000 nm using the same laser diode and a monochromator coupled with an amplified MIR detector (detector PCI-4TE-4-1 $\times$ 1, preamplifier PIP-DC-200M-F-M4, Vigo). All measurements are performed using glasses crushed into powder and at room temperature.

2.6. XRD analysis

An X-Ray Diffractometer (XRD) analyzer (PANalytical Empyrean) with Cu Kα X-ray radiation ($\lambda = 1.79$ Å) is used to identify the crystalline phases in the heat treated glasses. Data are collected from $2\theta = 20$ to $60°$ with a step size of $0.05°$. The samples were crushed into powder for the measurement.

2.7. Composition analysis

The composition and crystals formation of the heat treated glasses are investigated using a Scanning Electron Microscope (SEM, Crossbeam 540 Carl Zeiss) equipped with an Energy

Dispersive Spectroscopy (EDS/EDX) detector (Oxford Instruments X-MaxN 80). The samples are mounted on Al-stubs. The glasses are polished and then coated with a thin carbon layer prior to the SEM/EDX analysis. The detection limit of the EDX system was ± 0.5 at%.

3. Results and discussion

The table 1 reports the physical and thermal properties of the investigated glasses.

Table 1. Physical and thermal properties of the investigated glasses

Glass	ρ (g/cm^3) ± 0.02 g/cm^3	T_g (°C) ± 3°C	T_x (°C) ± 3°C	T_p (°C) ± 3°C	ΔT (°C) ± 6°C
GeY	4.55	642	821	842	179
GeZn	4.46	588	786	827	198
GeAl	4.30	630	790	816	160
GeTi	4.43	609	800	892	191

The density of the glasses decreases when replacing Y_2O_3 by ZnO, TiO_2 and Al_2O_3. The GeAl glass has the lowest density (4.30 g/cm^3) whereas the GeZn and GeTi glasses have similar density (4.46 and 4.43 g/cm^3 respectively). The substitution of Y_2O_3 by ZnO, Al_2O_3 and TiO_2 decreases the T_g, with the GeZn glass having the lowest one. Based on their thermal properties (Fig. 1(a)), the GeY and GeZn glasses are expected to have, respectively, the strongest and the weakest glass network among the investigated materials. Because of their large thermal stability parameter (ΔT), all glasses can be considered stable against crystallization and so good candidates to be drawn into fibers.
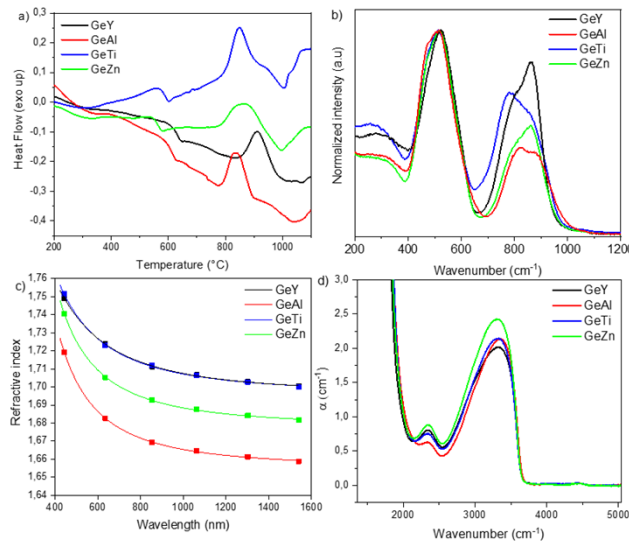
Fig. 1. a) DSC curves, b) Raman spectra, c) refractive index profiles, and d) IR absorption spectra of the investigated glasses

The normalized Raman spectra of the glasses are presented in Fig. 1(b). The Raman spectra observed are typical for germanate glasses. The bands are located in three different regions: 200 - 400 cm^{-1}, 420 - 600 cm^{-1} and 700 - 900 cm^{-1} [24]. The bands at 250 and 370 cm^{-1} can be assigned to the bending modes of Q^2 and Q^1 tetrahedra. The main band centered at 500-520 cm^{-1} can be attributed to the bending mode Ge [4]-O-Ge [4], the brackets referring to the coordination number of the atoms. The wavenumber position of this band gives information on the number

of tetrahedra forming the GeO_4 rings: in pure GeO_2, this band related to 6-membered GeO_4 rings is located at $420\,cm^{-1}$ [25] while this band is shifted to higher wavenumber when modifiers break the ring structure from 6- to 4- or 3-membered rings [24–27]. The bands in the region of 700-1000 cm^{-1} give information on the number of non-bridging oxygens (NBOs). Q^3, Q^2, Q^1 and $Q°$ units having 3, 2, 1 or 0 bridging oxygens respectively have typical Raman bands at 865, 780, 740 and 720 cm^{-1}, respectively [26]. The more these high frequencies bands are intense compared to the $500cm^{-1}$ band, the more the glass has NBOs.

It is known that the number of NBOs increases upon depolymerization of GeO_2 glass and Q^4- units transform in Q^3, Q^2, Q^1 and $Q°$ units and the whole Q-species envelope shifts to lower frequencies [26]. By comparing the intensity of the band at $520\,cm^{-1}$ and of the different Q-species in the range 700-1000 cm^{-1}, the GeY and GeAl glasses have the largest and lowest number of NBOs, respectively. Therefore, GeAl glass is expected to be the most polymerized glass and the GeY glass the most depolymerized glass which is also in agreement with the different intensities of the shoulder at ~465 cm^{-1}: GeAl and GeY glasses have the highest and the lowest relative intensity at ~465 cm^{-1}, respectively. GeTi glass has also a relatively high intensity at ~465 cm^{-1} (slightly higher than in GeY and GeZn glasses, and lower than in GeAl glass). For GeTi glass, the shift of the Q-species envelope to lower wavenumbers can be explained by formation of TiO_4 tetrahedra, which have Raman active modes at about 750 cm^{-1} [28]. A difference in the Q^3 band intensity ($865cm^{-1}$) compared to Q^2, Q^1, and $Q°$ bands indicate that Y and Zn are creating more NBOs than Ti and Al. GeTi and GeAl being the samples having the highest $465cm^{-1}$ band intensity, Al and Ti are acting more as network formers than Y and Zn. According to the Raman results the polymerization of the glasses decrease in the following order: GeAl→GeTi→GeZn→GeY.

The refractive index of the glasses measured at different wavelengths is shown in Fig. 1(c). Replacing Y_2O_3 by ZnO and Al_2O_3 tends to decrease the refractive index whereas the addition of TiO_2 at the expense of Y_2O_3 has no noticeable impact on the refractive index. The refractive index can be influenced by both the polarizability of the glass which depends on the number of electrons surrounding the atoms and the density of the glass [29]: if both the polarizability and the density of the glass increase, then the refractive index of the glass should increase. The GeY glass has the highest density with a high Y_2O_3 polarizability (polarizability of Y_2O_3 is 162 a.u [30]) so it is expected to possess a high refractive index. Ti has also a high polarizability (100 a.u.) and GeTi has a quite high density (the second highest considering the error bar), leading to a high refractive index too. GeAl and GeZn have respectively the lowest density and the lowest polarizability (38.67 a.u for Zn) leading them to be the glasses with the two lowest refractive indices (Al having a polarizability of 57.8 a.u).

The FTIR spectra of the studied glasses are shown in Fig. 1(d). The spectra exhibit broad bands which can be related to OH groups. The band at ~3300 cm^{-1} can be related to free, weakly associated hydroxyl groups. Although Feng et al. [31] attributed the shoulder at 2250 cm^{-1} to strongly associated hydroxyl groups, this shoulder was related to an anharmonic contribution of the bending mode at $2\delta_{OH}$ by Guery *et al*. [32]. The GeZn glass has the highest amount of OH groups while the GeY glass has the lowest amount of OH groups as expected from the network of the glasses: the more packed glass network (due to the higher number of 3-membered GeO_4-rings) the lower amount of OH groups. Similar reduction in OH groups due to addition of Y_2O_3 was reported by Xiao *et al*. [33].

Fig. 2(a) shows the absorption spectra of the different glasses in the range 300-700 nm. The typical absorption bands of Er^{3+} ions are visible, and they correspond to the transition of Er^{3+} ions from the ground state $^4I_{15/2}$ to the different excited states. The position of the band gap depends on the glass composition: the bandgaps of the GeTi glass is located at longer wavelength (α=15 cm^{-1} at 341 nm) compared to that of the GeZn glass (α=15 cm^{-1} at 303 nm), probably due to the TiO_4 tetrahedra formation [34]. The shift of the bandgap to higher wavelength has

already been observed by adding higher proportion of TiO_2 in glass [35]. Figure 2(b) and 2(c) display the 980 nm and 1550 nm Er^{3+} absorption bands. No significant differences either in the intensity of the absorption coefficient nor in the shape of the absorption bands are visible.
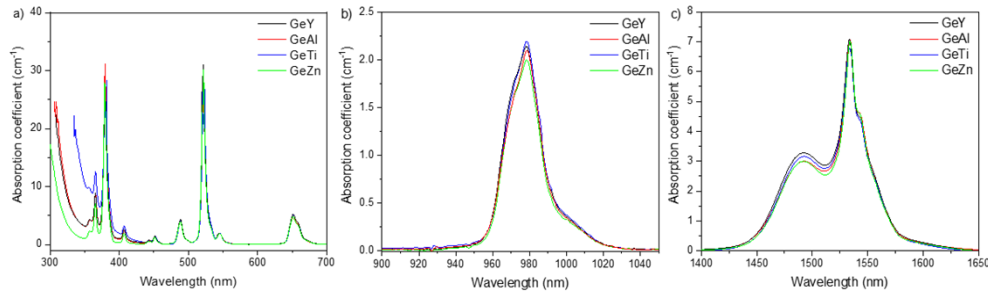
Fig. 2. Absorption spectra of the investigated glasses in a) visible, and at b) 980 nm and c) 1550 nm

As seen in Table 2, the absorption coefficients and cross-sections at 980 nm and 1530 nm are independent of the glass composition within the 10% error indicating that the local environment of Er^{3+} ions are similar in the investigated glasses. Thus, Y, Al, Zn and Ti are not expected to be in the coordination sites of Er^{3+} ions. The absorption cross-sections at 980 and 1530 nm are similar to those reported in other germanate glasses [36,37]. They are also similar to those reported in tellurite glasses [38–40] but higher than those reported in phosphate [41], silica and silicate glasses [42].

Table 2. Absorption coefficients (α_{abs}) and cross-sections (σ_{Abs}) at 980 nm and 1530 nm of the investigated glasses

Glass	$N_{Er}{}^{3+}$ (ions/cm^3) $(10^{20}) \pm 5\%$	α_{abs} (cm^{-1}) @980 nm	σ_{Abs} (cm^2) @980 nm $(10^{-21}) \pm 10\%$	α_{abs} (cm^{-1}) @1530 nm	σ_{Abs} (cm^2) @1530 nm $(10^{-21}) \pm 10\%$
GeZn	11.17	2.01	1.80	7.01	6.27
GeTi	11.11	2.20	1.98	6.78	6.11
GeAl	10.68	2.10	1.97	7.08	6.63
GeY	10.77	2.15	2.00	7.08	6.57

The normalized upconversion (transitions $^2H_{11/2} \rightarrow {}^4I_{15/2}$ at 524 nm, $^4S_{3/2} \rightarrow {}^4I_{15/2}$ at 544 nm, and $^4F_{9/2} \rightarrow {}^4I_{15/2}$ at 660 nm), NIR (transition $^4I_{13/2} \rightarrow {}^4I_{15/2}$ at 1.55 μm) and MIR (transition $^4I_{11/2} \rightarrow {}^4I_{13/2}$ at 2.7 μm) emission spectra of the Er^{3+} doped glasses under 980 nm excitation are presented in Fig. 3(a), b and c, respectively. All glasses exhibit similar emission bands confirming that Er^{3+} ions are localized in similar sites despite the differences in glass composition. Also, no significant changes of intensity of the UC, NIR and MIR emission have been observed at ± 15% in agreement with their similar OH content. Indeed, the link between OH content and energy transfer from Er^{3+} ions to quenching centers is well known in the case of the 1.55 μm emission [43].

The glasses were heat treated at (T_g + 20 °C) for 17 h and at their crystallization peak temperature (T_p) for 1 and 6 h. All heat treated glasses exhibit surface crystallization. The XRD patterns of the glasses prior to and after heat treatment are shown in Fig. 4(a-d). The as-prepared glasses show no crystal-related peaks prior to the heat treatment whereas sharp peaks appear afterwards confirming that crystallization occurs during the thermal treatment. The XRD patterns of the glasses exhibit peaks which can be attributed to $BaGa_2(GeO_4)_2$ [ICDD 04-009-4175] and $BaGe_4O_9$ [00-013-0295] crystals. Similar crystallization behavior with formation of $BaGe_4O_9$
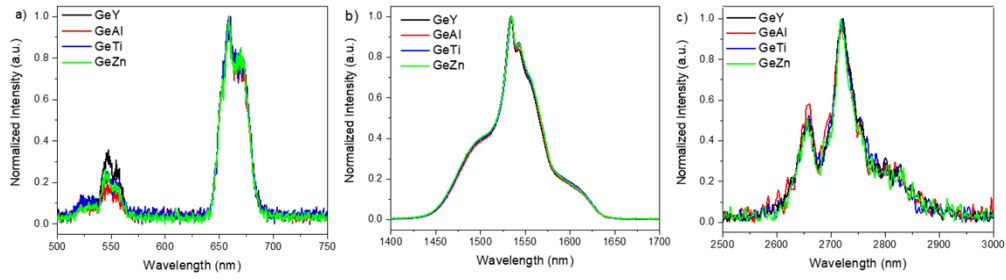
Fig. 3. Normalized a) upconversion and emission spectra centered at b) 1.5 μm (NIR) and at c) 2.7 μm (MIR) of the investigated glasses ($\lambda_{exc} = 980$ nm)
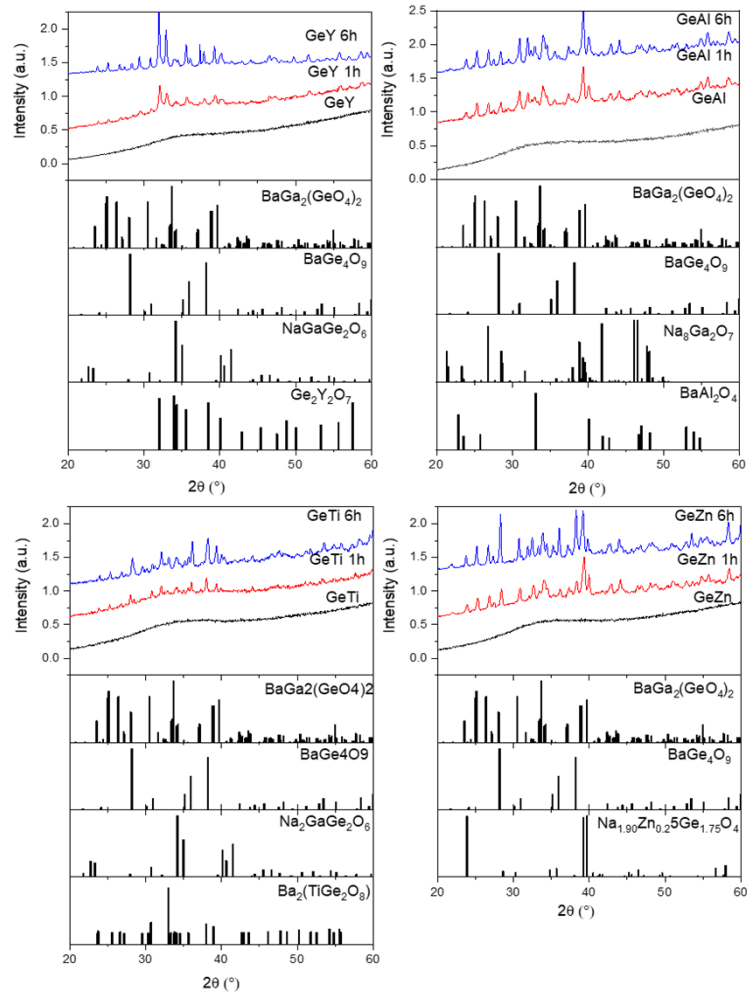
Fig. 4. XRD pattern of the a) GeAl, b) GeY, c) GeZn and d) GeTi glasses prior to (black) and after a heat treatment at ($T_g + 20$ °C) for 17 h and at T_p for 1 and 6 h.

crystal during a thermal treatment was reported for $70GeO_2$-$20BaO$-$10Ga_2O_3$ (mol%) glass [16]. The other peaks in the XRD pattern of the heat treated GeTi and GeY glasses could be assigned to $Na_2GaGe_2O_6$ [04-020-9808] crystal. $Ge_2Y_2O_7$ crystal [00-023-0272] is also expected in the heat treated GeY glasses and $Ba_2(TiGe_2O_8)$ crystal [05-001-0003] in the heat treated GeTi glasses. $Na_8Ga_2O_7$ [00-043-0794] and $BaAl_2O_4$ [04-013-9459] crystals are expected in the heat treated GeAl glasses and $Na_{1.90}Zn_{0.25}Ge_{1.75}O_4$ crystal in the heat treated GeZn glasses.

The presence of the crystals is confirmed in Fig. 5 which presents the SEM image of the cross-section of the heat treated glasses for 6 h. Surface precipitation of crystals with different shapes and chemistry depending on the glass composition is confirmed. The elemental mapping confirms the presence of Ge, Ga, Ba and Na rich crystals as suspected from the analysis of the XRD patterns. According to the elemental mapping, Er^{3+} doped crystals are expected in the heat treated GeY, GeTi and GeZn glasses. However, the homogeneous distribution of erbium in the Er elemental mapping in the heat treated GeAl glass might indicate that the crystals in this glass are Er^{3+} free.
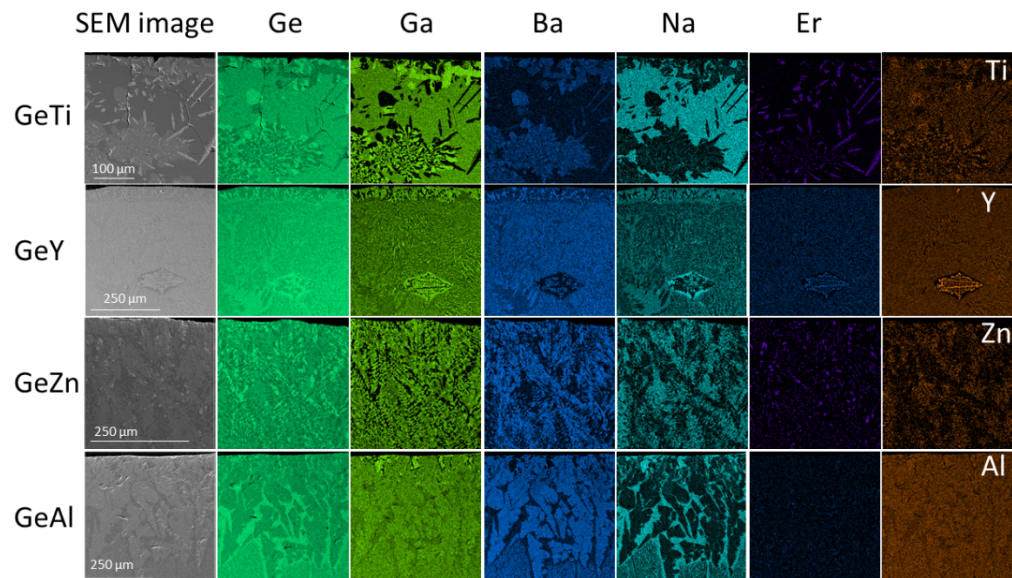
Fig. 5. SEM images and elemental mapping collected from the cross-section of the investigated glasses heat treated at (T_g + 20 °C) for 17 h and at T_p for 6 h

Figure 6 shows the upconversion (a, b, c, d), the NIR (e, f, g, h), and the MIR (i, j, k, l) spectra of the glasses prior to and after the heat treatment. The thermal treatment of the glasses increases the intensity of the UC and MIR emission and decreases the intensity of the NIR emission. These changes are the most pronounced for the GeY glass, while the least changes are observed for the GeAl glass. The shape of the UC and MIR bands, especially from the heat treated GeY, GeAl and GeZn glasses, also changes after heat treatment with the appearance of sharp peaks. The thermal treatment also increases the intensity of the UC and MIR emissions of GeY, GeTi and GeZn samples (considering the ±15% error bar). These changes in the spectroscopic properties confirm that some crystals contain Er^{3+} ions as suspected from EDX mapping analysis shown in Fig. 5. However, as the shape of the NIR emission remains broad after the thermal treatment, some Er^{3+} ions are suspected to remain in the amorphous part of the investigated heat treated glasses. The decrease in intensity of the NIR emission band might be also related to the decrease in the distance between the Er^{3+} ions in the glass after the crystallization which could also contribute to the increase in the intensity of the UC.
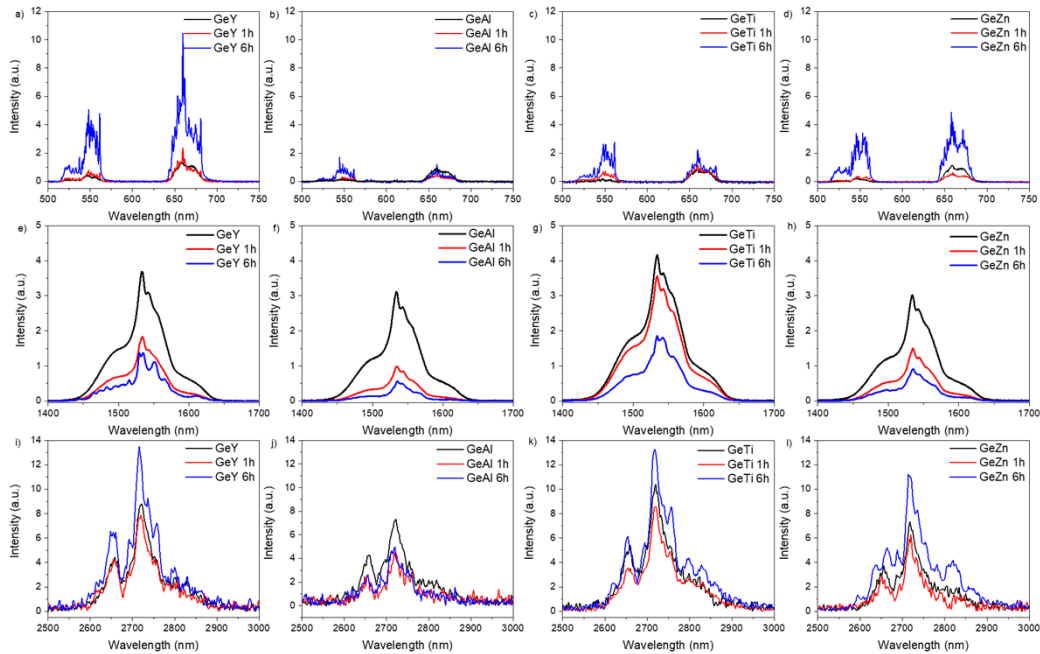
Fig. 6. The upconversion (a, b, c, d), the NIR (e, f, g, h), the MIR (i, j, k, l) emission spectra of the glasses prior to and after heat treatment at ($T_g + 20$ °C) for 17 h and at T_p for 6 h ($\lambda_{exc} = 980$ nm)

4. Conclusions

The impact of the replacement of Y_2O_3 by ZnO, TiO_2 or Al_2O_3 in Er-doped germanate glass on the spectroscopic properties and crystallization process is presented. Due to the difference in the composition of the glasses, the heat treatment leads to the formation of various crystals, even though two common crystals ($BaGa_2(GeO_4)_2$ and $BaGe_4O_9$) have been identified in all the glasses. The precipitation of Er-doped crystals becomes possible in the glasses with more depolymerized structure, namely GeZn, GeTi and GeY glasses. Spectroscopic data demonstrate that the heat treated GeZn, GeTi and GeY glasses are potential candidates as upconverters and for MIR applications.

Disclosures. The authors declare no conflicts of interest.

Data availability. Data underlying the results presented in this paper are not publicly available at this time but may be obtained from the authors upon reasonable request.

References

1. R. Moncorgé, L. D. Merkle, and B. Zandi, "UV-Visible Lasers Based on Rare-Earth Ions," MRS Bull. **24**(9), 21–26 (1999).
2. E. Snitzer, "Rare earth fiber lasers," J. Less-Common Met. **148**(1-2), 45–58 (1989).
3. A. B. Seddon, Z. Tang, D. Furniss, S. Sujecki, and T. M. Benson, "Progress in rare-earth-doped mid-infrared fiber lasers," Opt. Express **18**(25), 26704–26719 (2010).
4. S. D. Jackson, "Towards high-power mid-infrared emission from a fibre laser," Nat. Photonics **6**(7), 423–431 (2012).

5. H. Ebendorff-Heidepriem, T. C. Foo, R. C. Moore, W. Zhang, Y. Li, T. M. Monro, A. Hemming, and D. G. Lancaster, "Fluoride glass microstructured optical fiber with large mode area and mid-infrared transmission," Opt. Lett. **33**(23), 2861–2863 (2008).

6. Z. Zhao, B. Wu, X. Wang, Z. Pan, Z. Liu, P. Zhang, X. Shen, Q. Nie, S. Dai, and R. Wang, "Mid-infrared supercontinuum covering 2.0–16 µm in a low-loss telluride single-mode fiber," Laser Photonics Rev. **11**(2), 1700005 (2017).

7. R. Wang, X. Meng, F. Yin, Y. Feng, G. Qin, and W. Qin, "Heavily erbium-doped low-hydroxyl fluorotellurite glasses for 2.7 µm laser applications," Opt. Mater. Express **3**(8), 1127 (2013).

8. J. M. Florence, F. W. Glaze, C. H. Hahner, and R. Stair, "Transmittance of near-infrared energy by binary glasses," J. Am. Ceram. Soc. **31**(12), 328–331 (1948).

9. M. Dejneka and B. Samson, "Rare-Earth-Doped Fibers for Telecommunications Applications," MRS Bull. **24**(9), 39–45 (1999).

10. S. Shibata, T. Kanamoris, S. Mitachi, and T. Manabe, "Preparation and characteristics of PbF_2-AlF_3 and PbF_2-ZrF_4 glasses," Electron. Comm. Jpn. **63**(8), 94–99 (1980).

11. M Saad, "High purity fluoride glass synthesis: a review," Proc. SPIE **7228**, 72280G (2009).

12. A. R. Hilton, "Nonoxide chalcogenide glasses as infrared optical materials," Appl. Opt. **5**(12), 1877 (1966).

13. P. K. Singh and D. K. Dwivedi, "Chalcogenide glass: Fabrication techniques, properties and applications," Ferroelectrics **520**(1), 256–273 (2017).

14. P. L. Baynton, "Colour of Tellurite Glasses," Nature **176**(4484), 691–692 (1955).

15. J. de Clermont-Gallerande, S. Saito, M. Colas, P. Thomas, and T. Hayakawa, "New understanding of TeO_2–ZnO–Na_2O ternary glass system," J. Alloys Compd. **854**, 157072 (2021).

16. S. S. Bayya, J. S. Sanghera, I. D. Aggarwal, and J. A. Wojcik, "Infrared Transparent Germanate Glass-Ceramics," J. Am. Ceram. Soc. **85**(12), 3114–3116 (2004).

17. J.-P. Bérubé, A. L. Camus, S. H. Messaddeq, Y. Petit, Y. Messaddeq, L. Canioni, and R. Vallée, "Femtosecond laser direct inscription of mid-IR transmitting waveguides in BGG glasses," Opt. Mater. Express **7**(9), 3124–3135 (2017).

18. T. Wei, F. Chen, Y. Tian, and S. Xu, "Efficient 2.7µm emission and energy transfer mechanism in Er3 + doped Y_2O_3 and Nb_2O_5 modified germanate glasses," J. Quant. Spectrosc. Radiat. Transfer **133**, 663–669 (2014).

19. M. C. Rao, "Effect of Al_2O_3 on structural and luminescent properties of neodymium (Nd^{3+}) doped lead germanate glasses," Optik **172**, 509–518 (2018).

20. T. Wei, Y. Tian, F. Chen, M. Cai, J. Zhang, X. Jing, F. Wang, Q. Zhang, and S. Xu, "Mid-infrared fluorescence, energy transfer process and rate equation analysis in Er^{3+} doped germanate glass," Sci. Rep. **4**(1), 6060 (2015).

21. J. Pisarska, M. Sołtys, J. Janek, A. Górny, E. Pietrasik, T. Goryczka, and W. A. Pisarski, "Crystallization of lead-based and lead-free oxyfluoride germanate glasses doped with erbium during heat treatment process," J. Non-Cryst. Solids **501**, 121–125 (2018).

22. S. Kang, X. Xiao, Q. Pan, D. Chen, J. Qiu, and G. Dong, "Spectroscopic properties in Er^{3+}-doped germanotellurite glasses and glass ceramics for mid-infrared laser materials," Sci. Rep. **7**(1), 1–0 (2017).

23. Z. Zhao, B. Ai, C. Liu, Q. Yin, M. Xia, X. Zhao, and Y. Jiang, "Er^{3+} Ions-Doped Germano-Gallate Oxyfluoride Glass-Ceramics Containing BaF2 Nanocrystals," J. Am. Ceram. Soc. **98**(7), 2117–2121 (2015).

24. T. Skopak, S. Kroeker, K. Levin, M. Dussauze, R. Méreau, Y. Ledemi, T. Cardinal, E. Fargin, and Y. Messaddeq, "Structure and Properties of Gallium-Rich Sodium Germano-Gallate Glasses," J. Phys. Chem. C **123**(2), 1370–1378 (2019).

25. D. M. McKeown and C. I. Merzbacher, "Raman spectroscopic studies of BaO-Ga_2O_3-GeO_2 glasses," J. Non-Cryst. Solids **183**(1-2), 61–72 (1995).

26. E. I. Kamitsos, Y. D. Yiannopoulos, M. A. Karakassides, G. D. Chryssikos, and H. Jain, "Raman and Infrared Structural Investigation of $xRb_2O·(1 − x)GeO_2$ Glasses," J. Phys. Chem. **100**(28), 11755–11765 (1996).

27. G. S. Henderson and M. E. Fleet, "The structure of glasses along the Na_2O-GeO_2 join," J. Non-Cryst. Solids **134**(3), 259–269 (1991).

28. T. Fukushima, Y. Benino, T. Fujiwara, V. Dimitrov, and T. Komatsu, "Electronic polarizability and crystallization of K_2O–TiO_2–GeO_2 glasses with high TiO_2 contents," J. Solid State Chem. **179**(12), 3949–3957 (2006).

29. J. E. Shelby, "Introduction to glass science and technology, royal soc," Chemistry, Cambridge (2005).

30. P. Schwerdtfeger and J. K. Nagle, "2018 Table of static dipole polarizabilities of the neutral elements in the periodic table," Mol. Phys. **117**(9-12), 1200–1225 (2019).

31. X. Feng, S. Tanabe, and T. Hanada, "Hydroxyl groups in erbium-doped germanotellurite glasses," J. Non-Cryst. Solids **281**(1-3), 48–54 (2001).

32. G. Guery, T. Cardinal, A. Fargues, V. Rodriguez, M. Dussauze, D. Cavagnat, P. Thomas, J. Cornette, P. Wachtel, J. D. Musgraves, and K. Richardson, "Influence of Hydroxyl Group on IR Transparency of Tellurite-Based Glasses," Int. J. Appl. Glass Sci. **5**, 178–184 (2014).

33. Z. H. Xiao, A. X. Lu, and C. G. Zuo, "Structure and property of multicomponent germanate glass containing Y_2O_3," Adv. Appl. Ceram. **108**(6), 325–331 (2009).

34. K. I. Hussein, M. S. Alqahtani, K. J. Alzahrani, F. F. Alqahtani, H. Y. Zahran, A. M. Alshehri, I. S. Yahia, M. Reben, and E. S. Yousef, "The Effect of ZnO, MgO, TiO_2, and Na_2O Modifiers on the Physical, Optical, and Radiation Shielding Properties of a TeTaNb Glass System," Materials **15**(5), 1844 (2022).

35. N. Shimoji, T. Hashimoto, H. Nasu, and K. Kamiya, "Non-linear optical properties of Li_2O–TiO_2–P_2O_5 glasses," J. Non-Cryst. Solids **324**(1-2), 50–57 (2003).

36. Y. Yang, Z. Yang, B. Chen, P. Li, X. Li, and Q. Guo, "Spectroscopic properties and thermal stability of Er^{3+}-doped germanate–borate glasses," J. Alloys Compd. **479**(1-2), 883–887 (2009).

37. M. Cai, T. Wei, B. Zhou, Y. Tian, J. Zhou, S. Xu, and J. Zhang, "Analysis of energy transfer process based emission spectra of erbium doped germanate glasses for mid-infrared laser materials," J. Alloys Compd. **626**, 165–172 (2015).

38. P. Nandi and G. Jose, "Erbium doped phospho-tellurite glasses for 1.5μm optical amplifiers," Opt. Commun. **265**(2), 588–593 (2006).

39. I. Jlassi, H. Elhouichet, S. Hraiech, and M. Ferid, "Effect of heat treatment on the structural and optical properties of tellurite glasses doped erbium," J. Lumin. **132**(3), 832–840 (2012).

40. E. S. Yousef, "Er^{3+} ions doped tellurite glasses with high thermal stability, elasticity, absorption intensity, emission cross section and their optical application," J. Alloys Compd. **561**, 234–240 (2013).

41. N. Ojha, A. Szczodra, N. G. Boetti, J. Massera, and L. Petit, "Nucleation and growth behavior of Er^{3+} doped oxyfluorophosphate glasses," RSC Adv. **10**(43), 25703–25716 (2020).

42. W. L. Barnes, R. I. Laming, E. J. Tarbox, and P. R. Morkel, "Absorption and emission cross section of Er^{3+} doped silica fibers," IEEE J. Quantum Electron. **27**(4), 1004–1010 (1991).

43. Y. Yan, A. J. Faber, and H. de Waal, "Luminescence quenching by OH groups in highly Er-doped phosphate glasses," J. Non-Cryst. Solids **181**(3), 283–290 (1995).